ORIGINAL RESEARCH



Nitro-oxidized carboxycellulose nanofibers from moringa plant: effective bioadsorbent for mercury removal

Hui Chen · Sunil K. Sharma · Priyanka R. Sharma · Kai Chi · Eric Fung · Katherine Aubrecht · Ngonye Keroletswe · Samuel Chigome · Benjamin S. Hsiao •

Received: 24 March 2021/Accepted: 26 June 2021/Published online: 14 July 2021 © The Author(s), under exclusive licence to Springer Nature B.V. 2021

Abstract Mercury contamination in drinking water is a worldwide problem due to its severely harming effects on the human body. A nanostructured natural bioadsorbent, carboxycellulose nanofiber extracted from raw moringa plant using the nitro-oxidation method (termed NOCNF), capable of effectively remediating this problem has been demonstrated. Nitro-oxidation is a simple approach that can extract carboxylated nanocellulose directly from raw biomass. In this study, the produced NOCNF contained a large density of carboxylate groups on the cellulose surface (0.97 mmol/g), capable of removing Hg²⁺ ions by simultaneous electrostatic-interactions and mineralization processes. Using the Langmuir analysis, the adsorption results indicated that the highest

Hui Chen and Sunil K. Sharma have equal contribution

Supplementary information The online version contains supplementary material available at https://doi.org/10.1007/s10570-021-04057-5.

H. Chen · S. K. Sharma · P. R. Sharma (⊠) · K. Chi · E. Fung · K. Aubrecht · B. S. Hsiao (⊠) Department of Chemistry, Stony Brook University, Stony Brook, NY 11794-3400, USA e-mail: priyanka.r.sharma@stonybrook.edu

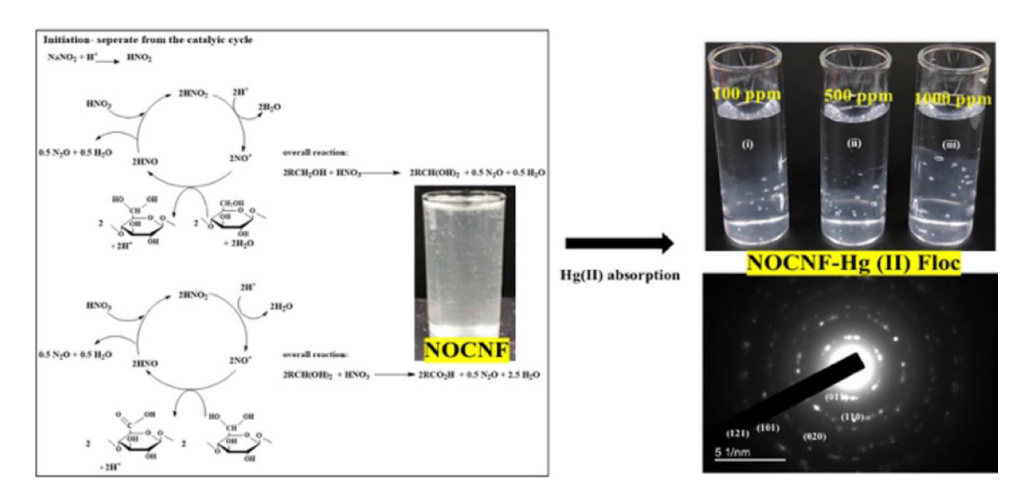
e-mail: benjamin.hsiao@stonybrook.edu

N. Keroletswe · S. Chigome Botswana Institute for Technology Research and Innovation, Private Bag 0082, Gaborone, Botswana 257.07 mg/g, which is higher than most of the reported values. The interactions between Hg²⁺ and NOCNF were further characterized by Fourier-transform infrared spectroscopy, scanning electron microscopy/energy dispersive spectroscopy (SEM/EDS), transmission electron microscopy with electron diffraction and wide-angle X-ray diffraction methods, suggesting the existence of two distinct removal mechanisms: predominant adsorption at low Hg²⁺concentrations (< 250 ppm) and predominant mineralization at high Hg^{2+} concentrations (> 1000 ppm). The applications of NOCNF were illustrated in both suspension form, as an adsorbent/coagulant, and dry powder form using filtration column. The results indicated that NOCNF in suspension exhibited a higher maximum removal efficiency of 81.6% as compared to the dry state of 74.3%. This work demonstrated the feasibility of extracting nanostructured adsorbents from biomass feedstocks to tackle the Hg²⁺ contamination problem in drinking water.

Hg²⁺ removal capacity of this NOCNF was



Graphic abstract Cellulose nanofibers, extracted from Moringa plant using the nitro-oxidation method, exhibit excellent adsorption capacity for Mercury (II) removal.

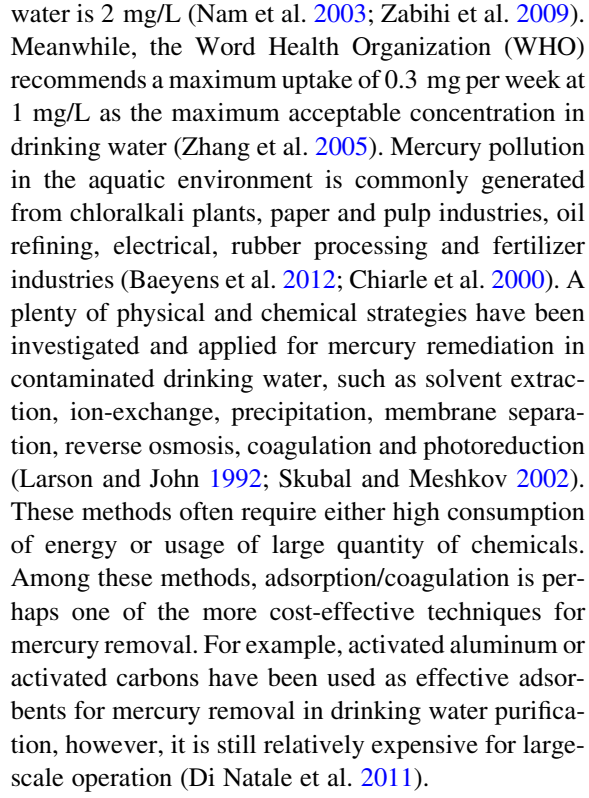


Keywords Nitro-oxidization · Cellulose nanofibers · Mercury removal · Moringa · Adsorption · Mineralization

Introduction

Mercury is a well-recognized harmful pollutant due to its carcinogenicity, mutagenicity and teratogenicity (Zhang et al. 2005). For example, high concentration of mercury in the human body can cause tyrosinemia, a disease associated with impairment of pulmonary and kidney function, chest pain and dyspnea. One main source of the mercury intake is through the consumption of contaminated fish. In 1956, a horrifying 'Minamata disaster' occurred in Japan, where people had unknowingly consumed shellfishes contaminated with mercury (Harada 1995; Rio and Delebarre 2003). Although it has been more than 50 years since the incident, many victims still suffer irreversible damage in their central nervous system. This is because mercury ions can bind to varying proteins in the nervous and renal systems, leading to permanent injury (Lai et al. 1993).

Due to the acute health threats to humans, the EPA permitted discharge limit of the total mercury amount in wastewater is 10 mg/L, where the limit for drinking



To tackle this problem, we argue that lignocellulosic biomass is an abundant and sustainable resource to develop cost-effective bio-adsorbent (Kim et al. 2015). In rural area, abundant agriculture waste can be



greatly utilized to treat contaminated water in a lower cost and more environmental-friendly way. In the past two decades, much attention has been given to develop nanocellulose in a broad range of water purification treatments because of its large surface areas and ample functional groups (Wang 2019). For example, several studies have been reported that cellulosic nanomaterials containing thiol, carboxyl, sulfonate, and phosphonate groups can all exhibit ability to adsorb positively charged contaminants, such as metal ions, dyes, and chemicals for water purification (Wang et al. 2013; Liu et al. 2016; Suman et al. 2015; Zhu et al. 2015; Sehaqui et al. 2016; Thakur and Voicu 2016; Chen et al. 2019; Sharma et al. 2020b).

Recently, a new method to extract carboxylated cellulose nanofiber from raw biomass using nitric acid (HNO₃) and sodium nitrite (NaNO₂) mixtures has been demonstrated by our team (we termed this nitrooxidation process or NOP) (Sharma et al. 2017b, 2018c). The method combines the steps of pulping (delignification) and cellulose oxidation. The proposed mechanisms of NOP are as follows. Nitric acid can facilitate the defibrillation process of raw biomass by degrading non-cellulosic components, such as lignin and hemicellulose, while the generation of NO⁺ ions (by reaction between HNO₃ and NaNO₂) can selectively oxidize the primary hydroxyl groups of the cellulose to introduce negatively charged surface to induce defibrillation. Compared with conventional methods, such as TEMPO-mediated oxidation and carboxymethylation processes, the NOP does not require any pretreatments such as alkali and bleaching to obtain cellulosic materials first, thus largely reducing the consumption of energy, water and chemicals. In addition, the effluent from this process can be neutralized into nitrogen salts as plant fertilizers (Sharma et al. 2017b). In our application studies, nitro-oxidized cellulose nanofibers (NOCNF) have been found as an effective adsorbent/coagulant to remove toxic metal ions such as cadmium (Sharma, Chattopadhyay, Sharma, et al. 2018a, b, c), lead (Sharma, Chattopadhyay, Zhan et al. 2018), and uranium (Sharma et al. 2017a, 2020a) from water.

In this study, we report that NOCNF, extracted directly from raw moringa plants by NOP, can also be an effective bioadsorbent for water remediation such as mercury removal. Moringa plant is native species in parts of Africa and Asia, and its products have well-known antifungal, antiviral, antidepressant, and anti-

inflammatory properties. In specific, seeds from Moringa tree have been shown to have unique water purification properties (Kalibbala et al. 2009). Here we investigate if the moringa plant itself can be a suitable feedstock for preparing the adsorbents. This is because the hemicellulose content of moringa plant is relatively high ($\sim 45\%$) (Melesse and Berihun 2013), which can facilitate the defibrillation process in NOP to produce cellulose nanofibers. For the mercury remediation study, we demonstrate the effectiveness of moringa-derived NOP as adsorbents in two different forms: suspension typical absorbent/coagulant, and dry form as adsorbent substrate in filtration column. The purpose of suspension/dry state adsorption tests is to investigate the absorption efficiency for mercury removal from drinking water in two sample formats. The NOCNF suspension format will be useful to treat contamination of local water sources with low Hg concentration since the transportation expense of the material will not be high; whereas the freeze-dried NOCNF (dry state) format will be useful to treat Hg contamination, when the concentration is high and the transportation cost needs to be considered. The study also examines the adsorption mechanisms of the mercury removal by the oppositely charged NOCNF. We demonstrate that at low Hg²⁺ concentrations (< 250 ppm), the removal process is mainly dominated by the electrostatic interactions between Hg²⁺ and COO on the NOCNF surface, where at high Hg^{2+} concentrations (> 1000 ppm), the removal process is dominated by the mineralization of HgO nanocrystals in the coagulated NOCNF scaffold.

Experimental

Materials

Crushed moringa straw samples, without any pretreatments, from Botswana was used as the biomass feedstock. Nitric acid (ACS reagent, 60%), sodium nitrite (ACS reagent \geq 97%), mercury acetate, sodium hydroxide, hydrochloric acid (36% assay) chemicals were purchased from the Fisher Scientific. All chemicals were used without any further purification.

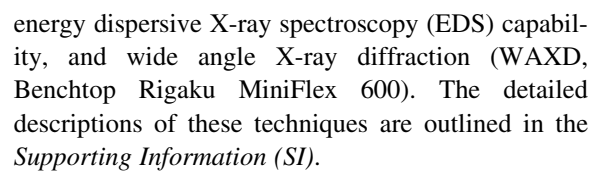


Extraction of NOCNF from moringa plant

NOCNF extraction from moringa feedstock were carried out using NOP with procedures similar to those reported earlier (Sharma et al. 2017b). In brief, 2 g of dried raw moringa sample was placed in a threeneck round bottom flask, where 28 mL nitric acid (60 wt.%, 0.365 mol) was added slowly to completely wet and immerse the biomass. Subsequently, 6.957 mmol of sodium nitrite (0.96 g) was added to the mixture under continuous stirring. Upon addition of sodium nitrite, red gases (NO_x) were formed. The mouths of flask were covered with glass stoppers immediately to stop gases from leaking. The reaction was performed at 40 °C for 16 h followed by quenching using 250 mL of distilled water to stop the reaction. The product was settled down under gravity and the supernatant was decanted off to remove the mixture of excessive acid, degraded lignin and oligosaccharides. The above step of decantation process was repeated for 2-3 times until the fibers started to suspend in water. After that, the fibers were centrifuged at 3000 rpm for 10 min. The step of centrifugation/washing with water was repeated till the pH of supernatant reached above 2.5. Then, the fibers were transferred to a dialysis bag (6-8 kDa) for dialysis until the conductivity of water reached below 5 µS. The extracted fibers contained carboxyl groups (COOH), which were subsequently converted to carboxylate groups (COO⁻) by treatment with 8% of sodium bicarbonate. The fibers were again introduced to dialysis until the conductivity of dialysis water reached below 5 µS. Finally, the fibers were fibrillated to nanocellulose by passing the 0.2 wt% fiber suspension through a high-pressure homogenizer at 250 bar for 1 cycle. The yield of NOCNF obtained was 50%.

Sample characterization

The raw moringa samples and extracted NOCNF were characterized using Fourier transform infrared spectroscopy (FTIR, PerkinElmer Spectrum One instrument-ATR conductometric mode), titration, thermogravimetric analysis (TGA, PerkinElmer STA-6000), transmission electron microscopy (TEM, FEI Tecnai G2 Spirit BioTWIN instrument), atomic force microscopy (AFM, Bruker Dimesion ICON scanning probe microscope), scanning electron microscopy (SEM, Zeiss LEO 1550 SFEG-SEM) with



The major chemical compositional analysis (i.e., cellulose, hemicellulose, lignin, ash, and extractives) of raw moringa sample and NOCNF was performed by the Celignis Company in Ireland. The analysis was in accordance with the US standard, i.e., NREL standard laboratory analytical procedure TP-510–42,623.(Sluiter et al. 2010) In brief, the following analytical procedures were carried out: (1) acid hydrolysis of samples, (2) determination of acid soluble lignin (ASL) using UV–Vis spectroscopy, (3) gravimetric determination of klason lignin (KL), and (4) chromatographic analysis of hydrolysate.

Mercury Remediation Study

Mercury Adsorption by NOCNF in Suspension

In this study, $\mathrm{Hg^{2+}}$ solutions with concentrations ranging from 2.5 to 1000 ppm were first prepared, where these solutions were subsequently mixed with a NOCNF suspension as an adsorbent/coagulant. In specific, 2 mL of heavy metal stock solution (2.5 to 1000 ppm) was slowly added with 2 mL of NOCNF suspension (0.40 wt%) in a test tube. Upon mixing, the floc, containing both aggregated Hg and NOCNF components, was formed and settled down to the bottom of the tube. The non-flocculated supernatant was then passed through a 0.22 μ m filter to remove any fiber residues, but not $\mathrm{Hg^{2+}}$ ions. The obtained solution was diluted before submitting for ICP-MS measurements.

Additionally, the effect of pH on the adsorption of ${\rm Hg^{2+}}$ by NOCNF was investigated. In this evaluation, 100 ppm ${\rm Hg^{2+}}$ solutions at different pH values: 3, 5, 7, 9 and 11, were prepared by adding 1 mol/L HCl or NaOH solution. Subsequently, 2 mL of NOCNF suspension was added to 2 mL of varying ${\rm Hg^{2+}}$ solutions. Similar to the above procedure, the non-floc portion were extracted, filtered through a 0.22 μ m filter and diluted 1000 times for ICP-MS analysis. The ICP-MS results were used to calculate the mercury removal efficiency of NOCNF.

The Hg²⁺ adsorption evaluation of NOCNF was performed by using the data obtained from the ICP-



MS analysis. In specific, the adsorption capacity at equilibrium (Qe) and equilibrium concentration of adsorbate (Ce) were calculated, where their relationship was evaluated by using both Langmuir and Freundlich isotherm models. The Langmuir model is based on the assumption of monolayer adsorption on the active site of the adsorbent, whereas the Freundlich model is based on the assumption of multilayer adsorption on the active site of the adsorbent. The Langmuir model can be expressed as follows.

$$\frac{Ce}{Qe} = \frac{Ce}{Qm} + \frac{1}{Qmb} \tag{1}$$

where Qm (the maximum adsorption capability) and b (the Langmuir constant) can be calculated from the intercept and the slope of the Ce/Qe versus Ce plot (Wang and Kuo 2007). In contrast, the Freundlich model can be expressed as follows.

$$\lg Qe = \frac{1}{n} \lg Ce + \lg Kf \tag{2}$$

where K_f and n are characteristic constants of the system (Cui et al. 2016).

Characterization of Hg-NOCNF Floc

The floc samples formed from the mixing of Hg²⁺ solutions and NOCNF suspension were characterized by different techniques including FTIR, TEM with electron diffraction, SEM/EDS and WAXD to determine the mechanisms of the mercury removal by NOCNF. In addition, the hydrophobicity of the floc sample was analyzed by an optical contact angle meter (CAM200, KSV instruments, LID), which is described in the *Supporting Information* (SI).

Preparation of filtration column for dry NOCNF adsorbent

The filtration column using freeze dried NOCNF samples was also carried out to test the $\mathrm{Hg^{2+}}$ removal efficiency. In specific, 3 g of dried NOCNF samples was used to fill a filtration column of 3 cm in diameter and 25 cm in length. Subsequently, a 100 ppm $\mathrm{Hg^{2+}}$ solution was added to the top of the column to initiate the test. A total number of 10 additions with an increment of 15 mL of $\mathrm{Hg^{2+}}$ solution for each addition was poured into the column, and the output filtrate obtained from bottom was collected and labeled

accordingly. The filtrate was diluted 1000 times and then submitted for ICP-MS measurements. The removal efficiency from the solid NOCNF form in the filtration column was compared with that from the dispersed NOCNF form in suspension.

Results and disscussion

Chemical composition analysis

Similar to other cellulose nanofibrils (such as TEMPO-CNF), the 0.4 wt% NOCNF suspension was translucent and showed viscous and gel-like behavior (as seen in the inset image in Fig. 1). This indicates that the nitro-oxidation process is an efficient pathway to defibrillate raw moringa plant even without pretreatments (or delignification step). The chemical compositions of the raw moringa plant and resulting NOCNF were quantitively characterized, and the results are shown in Fig. 1. It was seen that the holocellulose (cellulose and hemicellulose), lignin (acid soluble lignin (ASL) and klason lignin (KL)), ash and extractives contents of raw moringa were 60.3%, 24.78%, 6.48%, and 9.84%, respectively, while NOCNF exhibited a higher content of holocellulose (54.77%—mostly cellulose) and much lower content of lignin (4.0%). The significant decrease in the noncellulosic components after NOP confirmed its successful pulping function. We hypothesize that the residual lignin content in NOCNF might be due to the

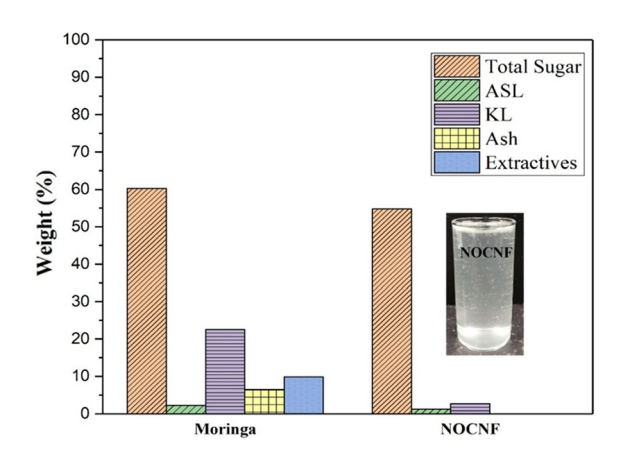


Fig. 1 Chemical compositions of raw moringa and extracted NOCNF (ASL: acid soluable lignin, KL: klason lignin). The inset image is the 0.4 wt% NOCNF suspension that exhibits the viscous and gel-like behavior)



presence of lignin-carbohydrate complexes, within which stable chemical bonds could resist the cleavage of β -O-4 ether bonds in polyphenolic units.

Figure 2 illustrates the likely mechanism of selective cellulose oxidation by the nitro-oxidation process, which is a revised version from the one we proposed earlier (Sharma et al. 2017b). In this mechanism, the reaction between HNO₃ and NaNO₂ generates HNO₂ and nitroxonium ions (NO⁺), which can selectively

attack primary hydroxyl group ($-CH_2OH$) of the cellulose unit at the C_6 position and produce $-CH(OH)_2$ group as the intermediate in the first oxidation circle. Subsequently, $-CH(OH)_2$ group can be continuously oxidized into carboxylic groups (-COOH) in the second oxidation circle. Overall, NO^+ as the oxidizing agent is gained and consumed during the reaction, where the end N-product is the mixture of NO_X gases. Although the exact compositions of NO_X

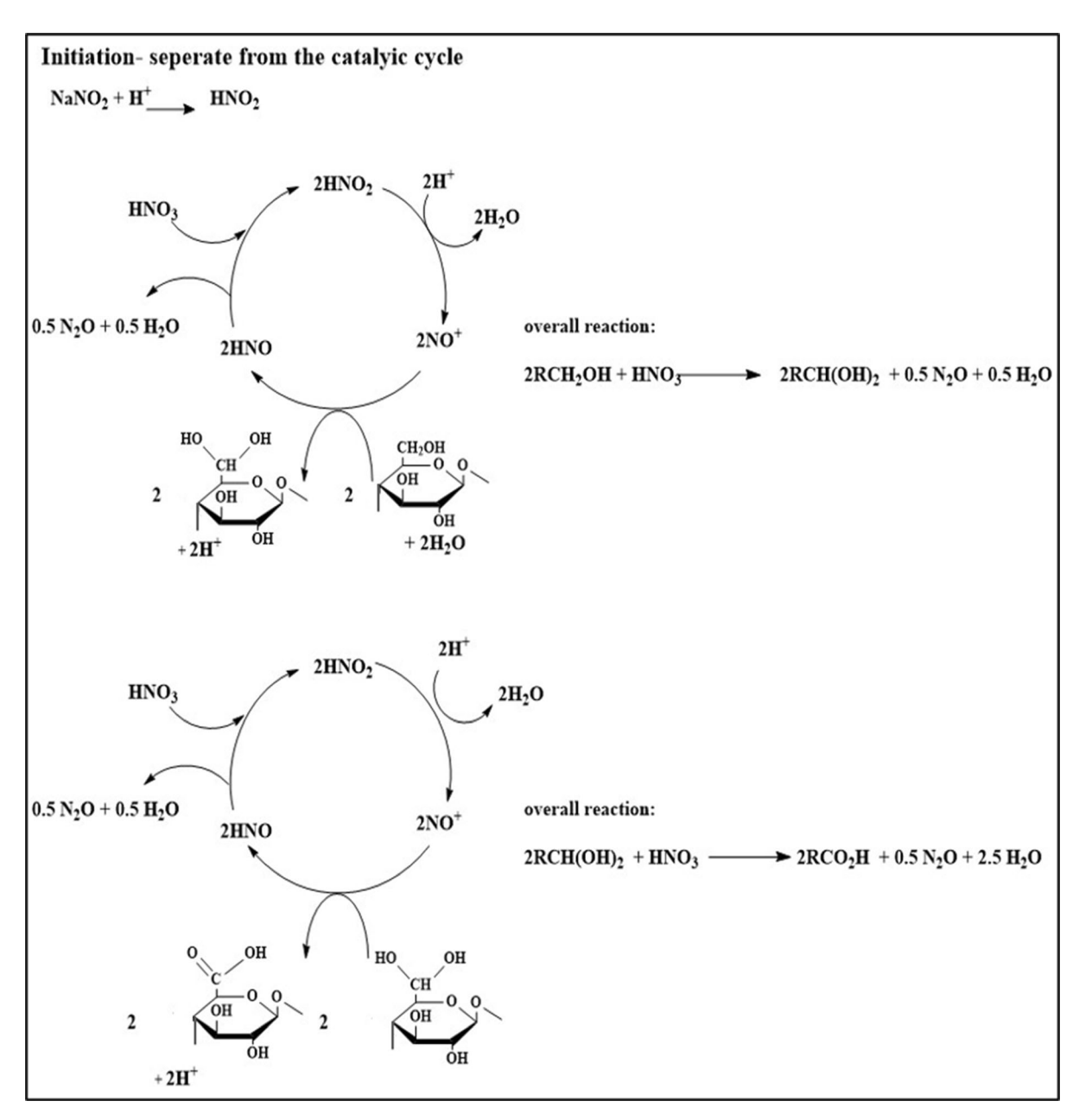


Fig. 2 Proposed cellulose oxidation mechanisms by the nitro-oxidation method



gases have not yet been determined, we believe the byproducts will contain three different gases: NO, NO_2 and N_2O . NO and NO_2 can be generated by the following reactions:

$$NO + 2HNO_3 \rightarrow 3NO_2 + H_2O$$

In addition, N_2O can be produced when HNO dissociates in water, as reported by Strojny (Strojny et al. 1971). In Fig. 2, we only indicate N_2O as a possible end N-product. Other gaseous products will also be possible, which will be experimentally verified in our future study.

Characterization of NOCNF

Figure 3(i) illustrates the FTIR spectra of raw moringa plant, extracted NOCNF and Hg-NOCNF floc after the remediation study. The FTIR spectrum of the moringa plant showed several distinctive peaks: 3328 cm⁻¹ corresponding to the -OH stretching and 2900 cm⁻¹ corresponding to the C-H symmetrical stretching in the cellulose unit; 1515 cm^{-1} due to the C = C symmetrical stretching in the aromatic lignin unit; and 1739, 1602, 1460, 1240, and 810 cm⁻¹ in the xylan unit. In the FTIR spectrum of NOCNF, it was seen that both OH stretching peak at 3328 cm⁻¹ and C-H stretching peak at 2900 cm⁻¹ became much sharper than those in moringa plant, confirming the hypothesis that some removal of lignin and hemicellulose components took place resulting in the dominant presence of cellulose scaffold. The delignification function of NOP was further verified by the near absence of the 1515 cm⁻¹ peak form the lignin unit. However, the hemicellulose peaks at 1739, 1602, 1460, 1240, and 810 cm⁻¹ remained visible, suggesting that the removal of hemicellulose in NOCNF is only partial. This is reasonable as the hemicellulose component acts as a crosslinker between cellulose elementary microfibrils, which may not be accessible by the oxidation process (Chi and Jeffery 2017). It is interesting to note that, the peak at 1602 cm⁻¹ due to the stretching motion in the carboxyl group was found to be notably increased in the NOCNF spectrum, verifying the modification of hydroxy group to carboxyl group in the anhydroglucose unit (probably at the C6 position) by NOP.

The WAXD pattern of the moringa plant in Fig. 3(ii) showed a cellulose I structure with 2θ angles at 14.8, 16.7, 22.7 and 34.7°, corresponding to (1–10), (110), (200) and (004) reflection planes, respectively. The peaks at 14.8 and 16.7° were overlapped, which needed to be deconvoluted to reveal individual intensity and position. This is a quite common in higher plants with cellulose I_{β} allomorph structure. For NOCNF, similar WAXD pattern was observed, suggesting the cellulose crystalline structure was maintained during nitro-oxidation, which only the defibrillation process proceeded. However, the peak positions of (1-10) and (110) were found to shift to lower 20 values (thus larger d-spacings), reflecting to the slight loosening of the crystalline structure due to cellulose oxidation. The crystallinity index (CI) values for the moringa plant and NOCNF were calculated by the peak height method (Segal's Equation, Supporting Information), and they were 61.2 and 67.3%, respectively. The slight increase in the crystallinity of NOCNF was mainly due to the reduction of amorphous, non-cellulosic components (lignin) during the nitro-oxidation process.

The thermogravimetric (TGA) and derivative thermogravimetric (DTG) profiles of raw moringa plant and NOCNF are shown in Figs. 3(iii) and 3(iv), respectively. The moringa plant showed the onset of thermal degradation (Tonset) at 174 °C with 9 wt% weight loss and the offset temperature (Toffset) was about 764 °C. In contrast, NOCNF exhibited Tonset at 136 °C with 15 wt% weight loss and Toffset at 802 °C. The lower Tonset value in NOCNF confirmed the removal of more thermally stable lignin component by nitro-oxidization, resulting in the exposure of holocellulose part that is more vulnerable to thermal decomposition. In addition, the earlier initialization of thermal degradation of NOCNF was probably due to the presence of anhydroglucuronic acid units (Sharma and Varma 2014b, 2014a), consisting of thermally unstable carboxyl groups.

The DTG curve of the moringa plant showed a primary peak at 302 °C, corresponding to the degradation of holocellulose moiety (Ornaghi et al. 2014; Zhang et al. 2013), and a secondary peak between 402 and 500 °C, related to the lignin moiety. In contrast, NOCNF displayed two primary peaks (260 °C and 300 °C), which are characteristics of oxidized nanocellulose, such as TEMPO-oxidized cellulose (Masruchin et al. 2019). The first peak is due to the



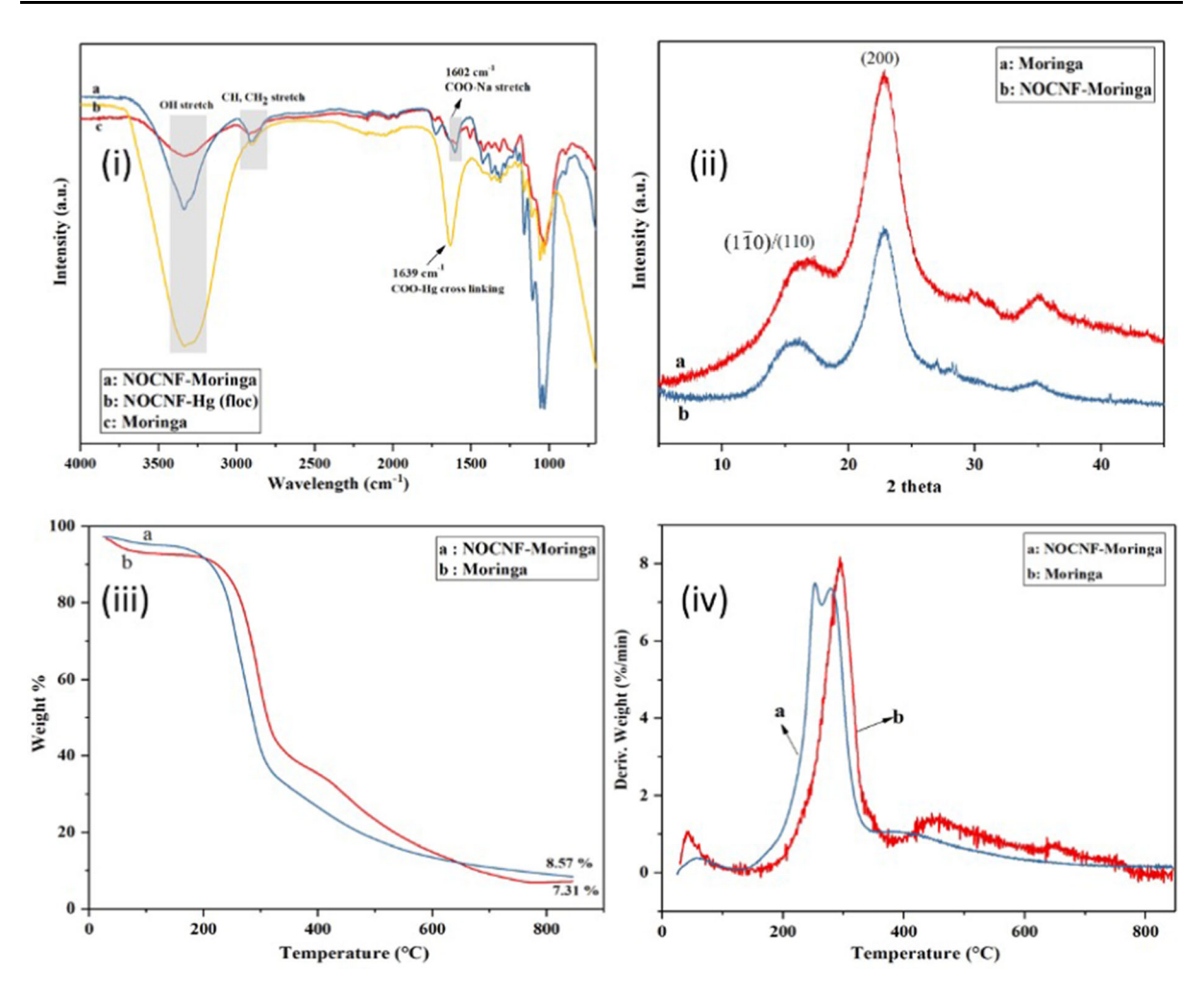


Fig. 3 Characterization of raw moringa plant, NOCNF and NOCNF-Hg floc: (i) FTIR of raw moringa plant (red curve), NOCNF (blue curve) and NOCNF-Hg floc (yellow curve); (ii) WAXD paterns of raw moringa plant (red curve) and NOCNF

(blue curve); (iii) TGA curves of raw moringa plant (red curve) and NOCNF (blue curve); (iv) Derivative Thermogravimetric (DTG) curve of raw moringa plant (red curve) and NOCNF (blue curve)

decomposition of the anhydroglucuronic acid units, where the surface carboxylate groups can initiate the decarbonation and decarboxylation reactions when subjected to heating. The second peak corresponds to the decomposition of residual un-modified cellulose moiety. In addition, a minor peak in the temperature range of 400–430 °C was observed in NOCNF, suggesting the lignin component was significantly removed during the nitro-oxidation process, which is consistent with chemical composition results in Fig. 1. Overall, the difference in thermal stability between moringa and NOCNF can be attributed to their surface chemistry and degree of polymerization (DP). After nitro-oxidation, a high amount of carboxyl groups is

generated on the surface of moringa cellulose, which can initiate the decarbonation and decarboxylation processes at low temperatures. In addition, under the influence of nitric acid pulping and cellulose oxidation by NOP, NOCNF's DP can be greatly reduced, resulting in more reducing ends and initiating sites for depolymerization and decomposition.

The carboxylate content of resulting NOCNF was determined by the conductimetric titration technique using Equation S2 in *Supporting Information*. The result indicated that the carboxylate content of NOCNF was 0.97 mmol/g, which is comparable to NOCNF derived from jute biomass as reported in our previous study (Sharma et al. 2020c). The surface



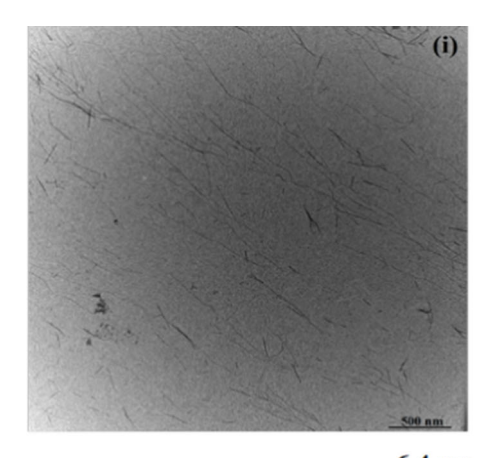
charge density of the NOCNF sample was also verified by the zeta potential measurement (see description in the *Supporting Information*), which yielded a negative zeta potential value of -59 mV confirming the abundant content of COO⁻ groups on the surface of NOCNF.

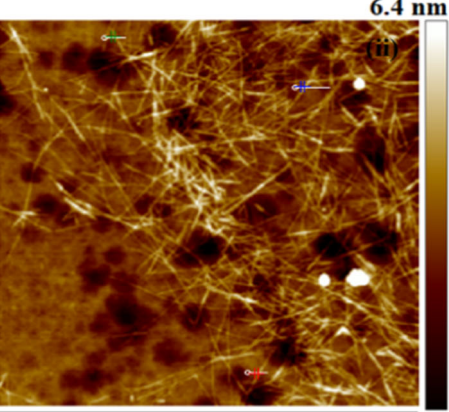
Morphological evaluation

A representative TEM image of NOCNF extracted from the moringa plant displayed the nanofibrous morphology as shown in Fig. 4(i). In this image, 20 individual fibers were identified and used to estimate the fiber length and fiber width, which were 250-300 nm and 10-12 nm, respectively. The AFM image (Fig. 4(ii)) presented similar nanofibrous morphology in NOCNF, where the height measurement indicated that the average fiber thickness was about 2.1 nm. This indicated that the extracted NOCNF possessed a ribbon shape instead of the circular-like fiber form. The representative SEM image of raw moringa sample is shown in Fig. 4(iii), indicating that the initial sample possessed a microscopic fiber form with width in the range of 20-100 µm and several millimeters in length. The morphological characterization of raw moringa fiber and NOCNF clearly confirmed the effective extraction of cellulose fibers from raw biomass using the nitro-oxidation process.

Characterization of NOCNF-Hg Floc

The FTIR spectrum of the NOCNF-Hg floc sample is illustrated in Fig. 3(i)c. In this spectrum, a shift of the carboxylate peak in NOCNF from 1602 cm⁻¹ to 1639 cm⁻¹ in the NOCNF-Hg floc was observed, probably due to the crosslinking between Hg²⁺ ions and carboxylate (COO⁻) groups of NOCNF. However, we note that the intensity of 1639 cm⁻¹ can also be attributed to the presence of the acetate group in the mercury acetate solution used in this study. Figure 5 illustrates the photographs of the floc formation by mixing 100, 500 and 1000 ppm of Hg^{2+} solutions with a NOCNF suspension under neutral condition. It was observed that white flocs were immediately formed, precipitated and settled down in the bottom of the tube in a very short period of time (less than 20 s). This indicated that the NOCNF in the suspension form is an excellent adsorption and coagulation agent, capable of





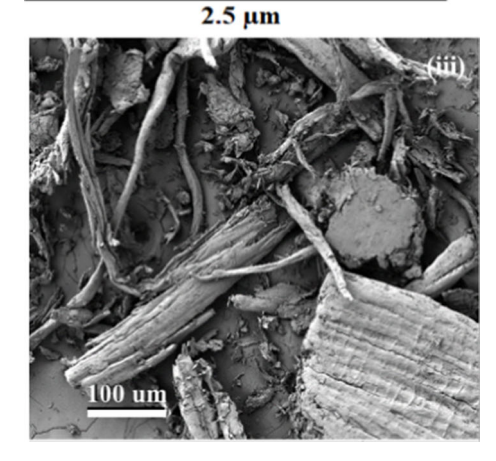


Fig. 4 Morphological characterization: (i) TEM and (ii) AFM images of NOCNF, (iii) SEM image of crushed moringa fibers

finding with Hg^{2+} ions, resulting in efficient removal of mercury contaminant.



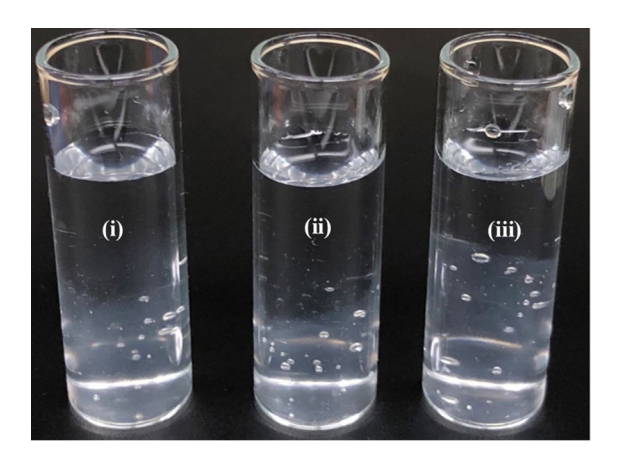


Fig. 5 Photographs of suspensions NOCNF-Hg floc, formed by mixing of (i) 100 ppm, (ii) 500 ppm and (iii) 1000 ppm of Hg²⁺ solutions with a 0.4 wt% NOCNF suspension

Mechanisms of Hg removal by NOCNF in suspension

To understand the interactions between Hg²⁺ ions and NOCNF in suspension, SEM and EDX images of floc samples formed with different Hg²⁺concentrations (250 ppm and 1000 ppm) are shown in Fig. 6. The two SEM images clearly exhibited the change in morphology of the NOCNF-Hg floc with different amounts of Hg²⁺. In Fig. 6(i), at a low concentration of Hg²⁺ (250 ppm), the floc surface was relatively uniform, where individual nanofibers could be identified. However, the presence of Hg was also apparent in the EDS spectrum. As the Hg²⁺ concentration increased to 1000 ppm, the floc surface became more

aggregated, but the individual fiber morphology disappeared. In fact, a few large aggregates were seen in otherwise a relatively smooth surface. These aggregates could be attributed to the mineralization of HgO on the NOCNF surface. The corresponding EDS spectrum confirmed the larger content of Hg in the NOCNF-Hg floc (1000 ppm) than that in NOCNF-Hg (250 ppm). In addition to the presence of Hg, EDS also showed the element of Na from the -COONa on NOCNF.

The different morphology of the NOCNF-Hg floc, containing varying amount of Hg adsorption, indicates that the adsorption mechanisms between the Hg²⁺ ions and NOCNF are quite different when the Hg²⁺ concentration changes. Based on the experimental results, we hypothesize that at low Hg²⁺ concentration (< 250 ppm), the Hg²⁺ ion behaves like an ionic cross-linking agent, capable of electrostatically interacting with two carboxylate groups (COO⁻) on the NOCNF surface. The binding of the Hg²⁺ ions and carboxylate groups would lead to the neutralization of NOCNF, resulting in further aggregation of NOCNF particles due to hydrophobic interactions. In the NOCNF-Hg floc, the adsorbed/anchored Hg moiety appeared to act as a nucleation site for the growth of mercury(II) oxide (HgO) nanocrystals on the surface of NOCNF. Most probably, the low pH value of the system can facilitate the growth of HgO nanocrystals because the acidic pH condition can hydrolyze mercury acetate and form unstable mercury hydroxide (Hg(OH)₂), which subsequently loses water and becomes HgO (Wang and Andrews 2005).

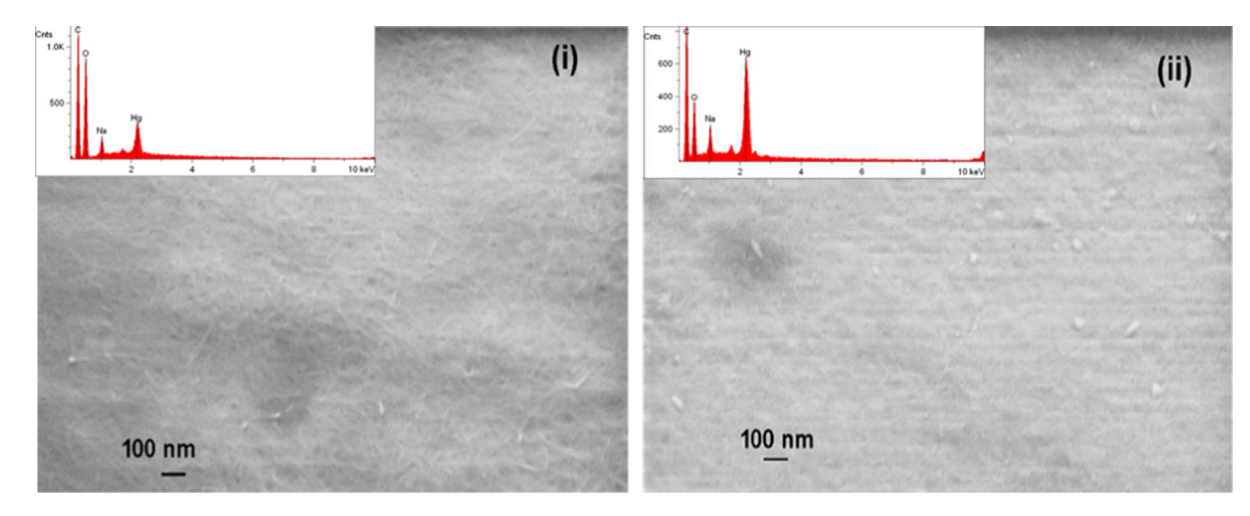
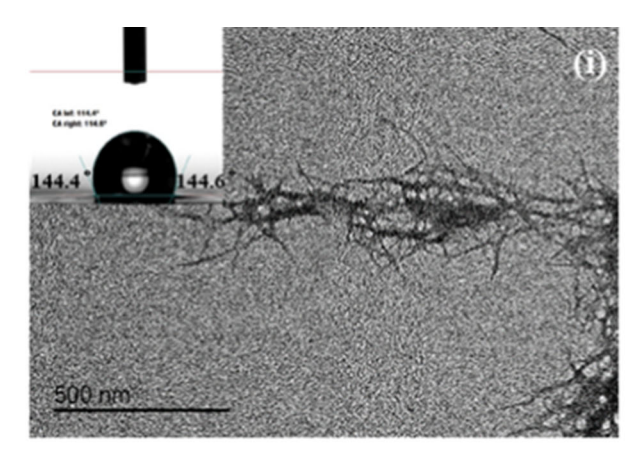


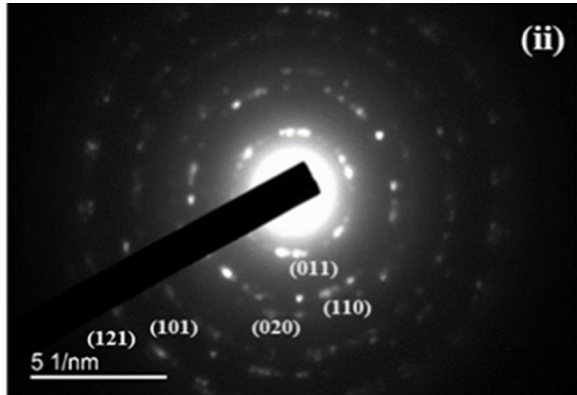
Fig. 6 SEM images with EDS spectra (the insert) of NOCNF-Hg floc formed by using i 250 ppm and ii 1000 ppm of Hg²⁺ solutions



The mineralization of HgO nanocrystals was confirmed by WAXD measurement of the floc (Fig. 7(-iii)), which will be explained later. The similar mineralization occurrence of nanocrystals in the CNF scaffold (such as lead hydroxide, cadmium hydroxide and uranium hydroxide) during remediation has also been reported earlier (Sharma et al. 2018b, 2018a, 2017a). To understand the HgO mineralization mechanism in this study, the pH values of the different Hg solution (at varying concentration)

before and after remediation using NOCNF were first measured, and the results are summarized in Table S1. It was seen that the pH value decreased upon the increase in the Hg concentration. For example, at the Hg concentration of 2.5 ppm, the pH value of the solution was 5.02; while at the concentration of 1000 ppm, the pH value was 3.44. The decrease in pH was due to the increase in acetate ions (CH₃COO⁻) in the solution, formed by dissociation of mercury acetate. Upon the addition of NOCNF, the same





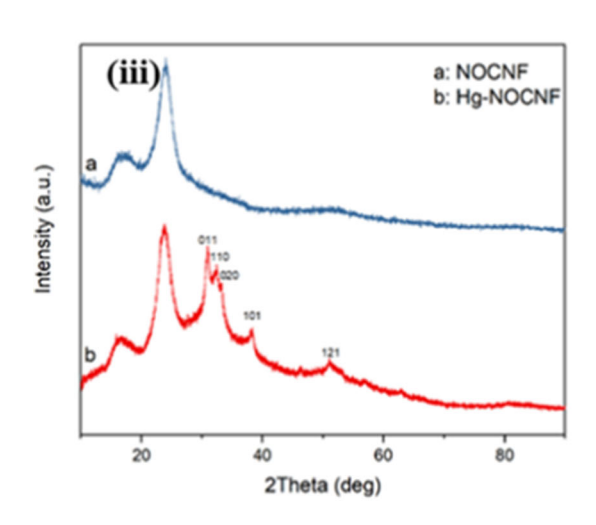




Fig. 7 Characterization of the NOCNF-Hg floc: i TEM image of the floc; the inset represents the contact angle of the floc, ii electron diffraction image of the floc, iii WAXD profiles of

NOCNF and NOCNF-Hg floc (formed by mixing of 0.32 wt% NOCNF suspension and 1000 ppm Hg²⁺ solution at the volume ratio of 1:1), and **iv** the setup of the filtration column



decreasing trend of the pH value was seen with the increase in Hg concentration, but the decrease in pH was stopped at 4.66 when 1000 ppm of Hg solution was used. Notably, no mineralization and precipitation were observed with increasing Hg concentration in the absence of NOCNF. The above finding indicates that NOCNF is playing a crucial role by providing the active site for adsorption and mineralization of Hg²⁺, leading to high removal efficiency against Hg²⁺ ions.

The hydrophobicity of the floc sample containing 1000 ppm of Hg²⁺ was analyzed by the contact angle measurement, and the results are shown in Fig. 7(i) (the inset image). This NOCNF-Hg floc sample was found to possess a contact angle of 114.5°, indicating that the Hg adsorption neutralized the charge on NOCNF resulting in a hydrophobic composite (the as extracted NOCNF has a contact angle about 38° (Sharma et al. 2018b). The WAXD measurement of the NOCNF-Hg floc sample was carried out to examine its crystal nature. The results are displayed in Fig. 7(iii), where the WAXD profile of NOCNF is also included for comparison. It was found that after remediation with 1000 ppm of Hg²⁺, additional diffraction peaks appeared at 2 of 30.8, 32.3, 33.4, 38.3 and 50.9°, which could be indexed as the (011), (110), (020), (101) and (121) lattice planes of HgO crystals (i.e., the orthorhombic phase of HgO with a space group of Imm2; JCPDS No. 72-1141) (Mohadesi et al. 2014). This evidence supports the growth of HgO nanocrystals in the NOCNF scaffold which is also in agreement with the SEM results from the floc sample at 1000 ppm of Hg concentration (Fig. 6(ii)). The TEM image of the floc sample with 1000 ppm of Hg concentration is shown in Fig. 7(i). Compared to the disperse fiber image of NOCNF (Fig. 4(i)), the NOCNF-Hg floc exhibited an aggregated form of nanofiber network containing inorganic nanocrystals shown as black dots in TEM. These black dots, uniformly dispersed in the fiber aggregate, are associated with the mercury oxide (HgO) particles. This was proven by the electron diffraction measurement of the floc sample, where the result is shown in Fig. 7(ii). The electron diffraction patterns of the floc sample showed five strong diffraction rings that could also be indexed as the (011), (110), (020), (101), (121) planes, as shown in WAXD (Fig. 7(iii)). We note that in the TEM study, no staining agent was used while preparing the sample; this ensured the absence of any other metal ions except merury.



Assessment of Hg²⁺ adsorption mechanism by NOCNF suspension

The behavior of Hg²⁺ adsorption by NOCNF was evaluated in the Hg concentration range of 2.5 ppm to 1000 ppm. The ICP-MS results were used to calculate the Qe value (i.e., the experimental adsorption capacity of NOCNF) and Ce/Qe ratio (i.e., the original Hg²⁺ concentration of NOCNF divided by the experimental adsorption capacity of Hg²⁺ ions at equilibrium per gram of NOCNF in suspension). It was found that the adsorption efficiency of Hg²⁺ by NOCNF decreased from 88.5 to 47.2% when the Hg concentration increased from 2.5 to 1000 ppm. Meanwhile, the experimental capacity raised from 0.55 mg/g to 117.9 mg/g. Using Eq. 1, the plot of Ce/Qe versus Ce was fitted with the Langmuir adsorption model, and the result is illustrated in Fig. 8(i). The value of Oe was calculated by multiplying the adsorption efficiency of NOCNF by the ideal adsorption capacity of NOCNF. The results of the ideal adsorption capacity and the experimental capacity of NOCNF are summarized in Table S2 in the Supplementary Information. In addition, the Freundlich adsorption model was also employed to predict the isotherm of Hg^{2+} remediation process. The plot of lg(Qe) versus lg(Ce)fitted by the Freundlich equation (Eq. 2) is shown in Fig. 8(ii). The fitting parameters, such as the slope and R square value, of these two models are summarized in Table 1. Both models exhibited very high R square values: 0.9946 for the Langmuir model, and 0.9951 for the Freundlich model. These results suggest that the adsorption mechanism cannot truly be differentiated based on the different model analysis. Nevertheless, from the analysis of the Langmuir model, the *Qm* value (the maximum adsorption capacity of the adsorbent) could be calculated, i.e., 257.07 mg/g, which is higher than most adsorbents reported (Tran et al. 2015; Anbia and Amirmahmoodi 2016; Puanngam and Unob 2008; Guo et al. 2017; Sajjadi et al. 2018; Anoop Krishnan and Anirudhan 2002).

Effect of pH and Time on Hg^{2+} remediation by NOCNF suspension

The pH effect on Hg²⁺ remediation was carried out to assess the removal efficiency of NOCNF in suspension, and the results are summarized in Table S3 in *Supporting Information* and in Fig. 8(iii). It was

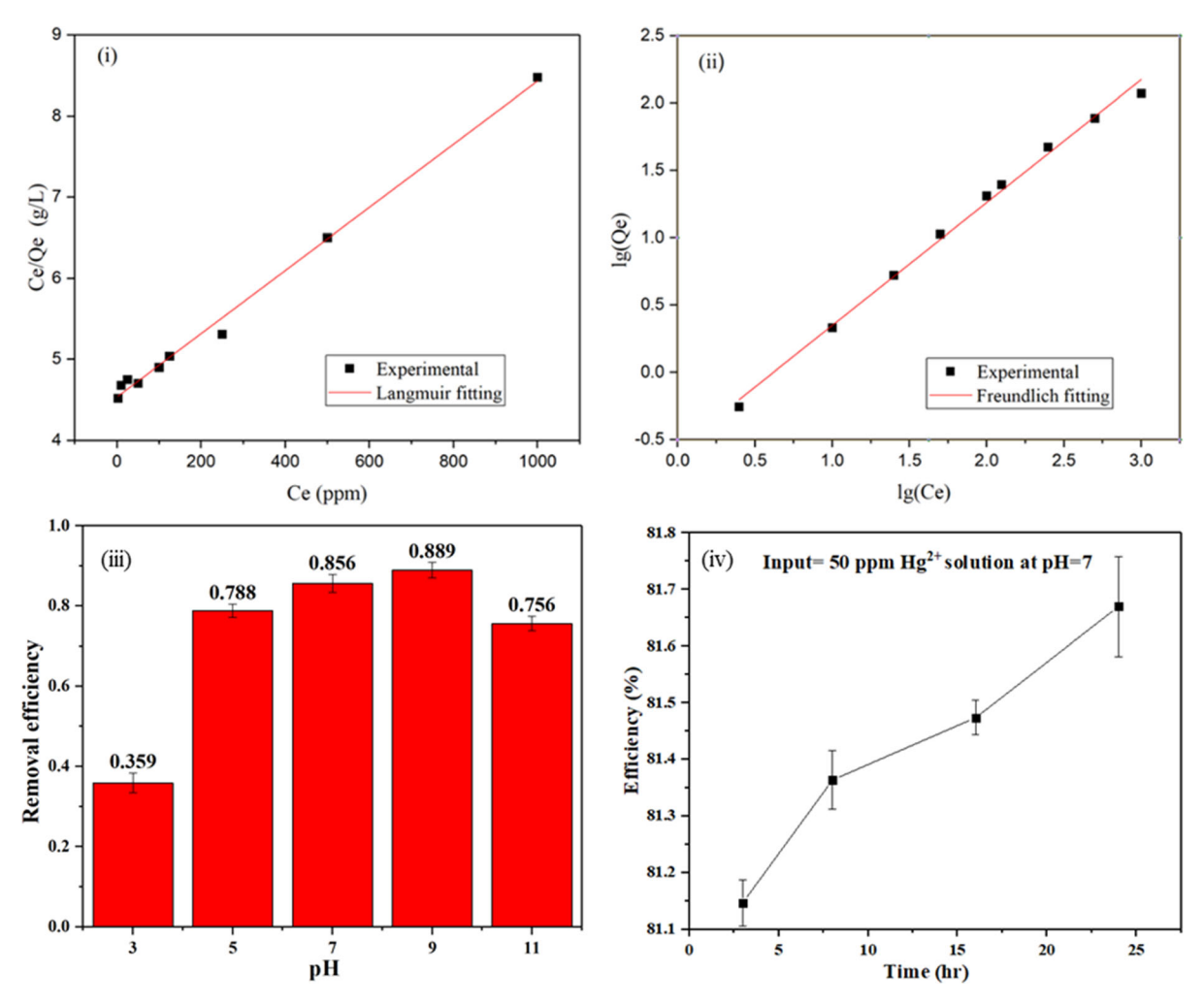


Fig. 8 (i) The ${\rm Hg^{2+}}$ adsorption data by using the NOCNF suspension as an adsorbent (the ${\rm Hg^{2+}}$ concentration was ranged between 2.5 to 1000 ppm) analyzed by the Langmuir model, (ii) the adsorption data analyzed by the Freudlich model, (iii) the

effect of pH on the removal efficiency and; (iv) the effect of time on the ${\rm Hg^{2+}}$ removal efficiency by NOCNF at 100 ppm ${\rm Hg^{2+}}$ concentration at pH = 7

Table 1 Summary of the Langmuir and Freundlich fitting model parameters

	Langmuir		Freundlich	
Equation	y = 0.00389x + 4.538		y = 0.91338x-0.565	
\mathbb{R}^2	0.9946		0.9951	
Parameters	b	Qm (mg/g)	n	K_f
Value	0.00086	257.07	1.095	3.673

observed that the removal efficiency increased to 88.9% when the pH value increased from 3 to 9. The

reason that at pH = 9, the highest removal efficiency was obtained is because the maximum negative charge density of NOCNF could be induced by the deprotonation of carboxyl group (COO $^-$) at alkaline conditions. With a further increase in the pH value to 11, NOCNF showed a decrease in the removal efficiency to 75.6%. This is because the further increase in pH, the condition might start to degrade NOCNF. In contrast, the removal efficiency of NOCNF at pH = 3 was only 35.9%,. This is because the acidic conditions could protonate the carboxylate groups on the NOCNF surface, resulting in an acid form (COOH) with less binding sites available to interact with the Hg²⁺ ions. The above study clearly indicates the pH-dependent



characteristic of NOCNF for mecury removal, as the NOCNF suspension can be considered as a weak polyelectrolyte due to the carboxylate group on the particle surface.

The effect of time on the Hg²⁺ remediation by NOCNF suspension was also evaluated, and the results are shown in Fig. 8(iv). It was found that there was no significant change in the removal efficiency when the experiments were performed between 3 and 24 h. The removal efficiency was stabilized between 81.1 and 81.6%, indicating that the removal of Hg²⁺ by NOCNF took place mainly in the initial hours of the remediation study. This study shows that a swift remediation process can be achieved by using NOCNF suspension as a mercury removal agent.

Comparison with other adsorbents

The comparison of the maximum adsorption capacity (*Qm*) of different adsorbents for mercury removal is listed in Table 2. Compared to nanomaterials, such as thiol and hydroxyl containing montmorillonite (Tran et al. 2015), nanoporous carbon grafted with surfacants (Anbia and Amirmahmoodi 2016), and chemically-modified MCM-41 and silica gel (Puanngam and Unob 2008), NOCNF extracted from moringa plants showed the highest maximum adsorption capacity value of 257 mg/g in the Hg concentration range of 2.5–1000 ppm. In Table 2, some natural biomaterials, such as coconut husk (Guo et al. 2017) and activated

carbon (Sajjadi et al. 2018) prepared from different sources have also been included. Among them, one activated carbon presented very good maximum adsorption capacity value of 202 mg/g, although in a very narrow Hg concentration range of 2.5–4.5 ppm. The activated carbon (Anoop Krishnan and Anirudhan 2002) prepared from bagasse pith also exhibited good maximum adsorption capacity of 172 mg/g in a wider Hg concentration range of 50-1000 ppm. But these values are still smaller than that of NOCNF. We believe the good performance of NOCNF should be independent of the biomass source used. The remarkable mercury removal property of NOCNF in suspension is due to its high surface area, large carboxylate concentration and unique scaffolding capability to induce HgO mineralization.

Filtration column using Freeze-Dried NOCNF

NOCNF suspensions were also freeze-dried into dry powder samples as adsorbent materials in filtration column for the evaluation of mercury removal. In this study, 3 g of dried NOCNF sample was packed into a column of 15 cm in length. Subsequently, 100 ppm of Hg²⁺ solution was passed through the column slowly by gravity. The output Hg²⁺ solution was collected and tested by the ICP-MS technique, where the results are shown in Table 3. It was seen that the removal efficiency achieved by this gravity-driven column in the first pass of the study was 74.3%, but the removal

Table 2 Comparison of the maximum adsorption capacity of varying adsorbents reported in the literature and NOCNF in this study against the Hg^{2+} removal

Adsorbents	Maximum adsorption capacity Qm (mg/g)	Adsorption range (ppm)	Reference
Thiol and hydroxyl containing montmorillonite	8.57	< 100	(Tran et al. 2015)
Nanoporous carbon impregnated with surfactants	8.9	10–200	(Anbia and Amirmahmoodi 2016)
MCM-41-NH-L	152	100-800	(Puanngam and Unob 2008)
Silica gel	140	100-800	(Puanngam and Unob 2008)
Coconut husk	44.9	40-450	(Guo et al. 2017)
Activated carbon from pistachio wood waste	202	2.5–45	(Sajjadi et al. 2018)
Activated carbon from bagasse pitch	172	50–1000	(Anoop Krishnan and Anirudhan 2002)
NOCNF from moringa plant	257.1	2.5-1000	This study



Table 3 Results from filtration column using NOCNF for Hg²⁺ removal

Column label	Input concentration (ppm)	Filtrate ICP-MS concentration (ppb)	Filtrate concentration (ppm)	Efficiency
1	100	25.7	25.70	0.743
2	100	26.5	26.50	0.735
3	100	31.1	31.10	0.689
4	100	31.6	31.60	0.684
5	100	33	33.00	0.670
6	100	34.8	34.80	0.652
7	100	35.5	35.50	0.645
8	100	40.4	40.40	0.596
9	100	42.5	42.50	0.575
10	100	46.7	46.70	0.533

efficiency began to decrease upon further addition of the Hg²⁺ solution. With the total passing of 150 mL filtrate (10 additions of 15 ml Hg²⁺ solution) through the column, the removal efficiency was found to be 53.3%. The decrease in the removal efficiency of the column was due to the saturation of carboxyl groups on the NOCNF surface through binding with Hg²⁺ ions. It was seen that the adsorption results from the use of NOCNF suspension indicated the removal efficiency of 81.6% at the Hg concentration of 100 ppm (Table S2 in Supporting Information), which is higher than the removal efficiency by using solid NOCNF in filtration column. This can be explained as follows. During freeze drying process, the aggregation of nanocellulose can occur due to the increasing interfibrillar interactions (van der Waal forces and hydrogen bonding), leading to reduced surface area and decreasing binding sites for Hg²⁺ ions in the NOCNF scaffold. In the filtration column application, the primary adsorption mechanism is dominated by the electrostatic interactions between carboxylate groups and the Hg²⁺ ions, where the mineralization process probably does not occur. To improve the total removal efficiency of the column, one needs to increase the total carboxylate content of the adsorbent by raising: (1) the degree of CNF oxidation, (2) the total loading of NOCNF, and (3) the surface area of NOCNF. Furthermore, we argue although the removal efficiency of solid NOCNF is not as good as NOCNF in suspension, the transportation cost of the formal may be much more cost-effective than the latter.

Conclusions

This work demonstrates an effective nanocellulosebased adsorbent system (in suspension or solid form) for mercury removal that was developed from untreated moringa plant using the nitro-oxidation method. The structure, property and functionality of the resulting NOCNF was thoroughly characterized by SEM, TEM, AFM, FTIR, WAXD, TGA and DTG techniques. The nitro-oxidation method appears to be a useful approach that can extract nanocellulose adsorbents from many other raw biomass sources. The present mercury remediation study using NOCNF comprises of three major activities to investigate (i) the adsorption mechanism of NOCNF in suspension against Hg²⁺ ions; (2) the effects of pH and time on the adsorption capacity and removal efficiency of Hg²⁺ by NOCNF; and (3) the deployment of NOCNF suspension as an adsorbent/coagulant system, and of solid NOCNF adsorbent in filtration column. In the mechanism study, it was found that at low Hg²⁺ concentrations (< 250 ppm), the removal mechanism was dominated by electrostatic interactions between Hg²⁺ and COO⁻ on the NOCNF surface; at high Hg²⁺ concentrations (> 1000 ppm), the removal mechanism was dominated by the mineralization process of HgO crystal formation in the NOCNF scaffold. As a result of the mineralization, the maximum adsorption capability of NOCNF for the Hg^{2+} removal at pH = 7 was 257.07 mg/g, which was the highest among all mercury adsorbents reported thus far. Finally, we observed that the removal efficiency by the NOCNF suspension was higher than that of the solid NOCNF



8626 Cellulose (2021) 28:8611–8628

adsorbent in filtration column as expected. However, the practical depolyment value for each system will depend on the detailed techno-economic assessment of the technology that is also location dependent.

Acknowledgments The financial support for this work was provided by a grant from the Polymer Program of the Division of Materials Science in the National Science Foundation (DMR-1808690). The authors thank Drs. Chung-Chueh Chang and Yuan Xue at the Advanced Energy Research and Technology Center in Stony Brook University for the assistance of the TGA, TEM and AFM measurements, and Ms. Katie Wooton at the Facility for Isotope Research and Student Training in Stony Brook University for the assistance of the ICP-MS analysis.

Author contributions All authors contributed to the study conception and design. Materials were provided by NK and SC from Botswana Institute for Technology Research and Innovation; Material preparation, data collection and analysis were performed by HC and EF. The first draft of the manuscript was written by HC and all authors commented on previous versions of the manuscript. All authors read and approved the final manuscript; Authors have no conflicts of interest; Data and material are all transparent.

Funding The financial support of this study is provided by the National Science Foundation (DMR-1808690).

Data availability The experimental data and materials are available upon request.

Declarations

Conflict of interest There are no conflicts of interest and competing interests among the authors of this study.

References

- Anbia M, Amirmahmoodi S (2016) Removal of Hg (II) and Mn (II) from aqueous solution using nanoporous carbon impregnated with surfactants. Arabian J Chem 9:S319–S325. https://doi.org/10.1016/j.arabjc.2011.04.004
- Anoop Krishnan K, Anirudhan TS (2002) Removal of mercury(II) from aqueous solutions and chlor-alkali industry effluent by steam activated and sulphurised activated carbons prepared from bagasse pith: kinetics and equilibrium studies. J Hazard Mater 92:161–183. https://doi.org/10.1016/S0304-3894(02)00014-6
- Baeyens W, Ebinghaus R, Vasiliev O (2012) Global and regional mercury cycles: sources, fluxes and mass balances. Springer, Berlin
- Chen H, Sunil KS, Priyanka RS, Heidi Y, Ken J, Benjamin SH (2019) Arsenic(III) removal by nanostructured dialdehyde cellulose–cysteine microscale and nanoscale fibers. ACS Omega 4:22008–22020. https://doi.org/10.1021/acsomega.9b03078

- Chi K, Jeffrey MC (2017) The influences of added polysaccharides on the properties of bacterial crystalline nanocellulose. Nanoscale 9:15144–15158. https://doi.org/ 10.1039/C7NR05615J
- Chiarle S, Ratto M, Rovatti M (2000) Mercury removal from water by ion exchange resins adsorption. Water Res 34:2971–2978. https://doi.org/10.1016/S0043-1354(00)00044-0
- Cui G, Min L, Ying C, Wei Z, Jiangqi Z (2016) Synthesis of a ferric hydroxide-coated cellulose nanofiber hybrid for effective removal of phosphate from wastewater. Carbohydr Polym 154:40–47. https://doi.org/10.1016/j.carbpol. 2016.08.025
- Di Natale F, Erto A, Lancia A, Musmarra D (2011) Mercury adsorption on granular activated carbon in aqueous solutions containing nitrates and chlorides. J Hazard Mater 192:1842–1850. https://doi.org/10.1016/j.jhazmat.2011.07.021
- Guo YF, Zhuo W, Zhou X, Renbi B (2017) Removal of mercury (II) from aqueous solution with three commercial raw activated carbons. Res Chem Intermed 43:2273–2297. https://doi.org/10.1007/s11164-016-2761-y
- Harada M (1995) Minamata disease: methylmercury poisoning in Japan caused by environmental pollution. Crit Rev Toxicol 25:1–24. https://doi.org/10.3109/10408449509089885
- Kalibbala HM, Olle W, Hawumba TJ (2009) The impact of Moringa oleifera as a coagulant aid on the removal of trihalomethane (THM) precursors and iron from drinking water. Water Sci Technol Water Supply 9:707–714. https:// doi.org/10.2166/ws.2009.671
- Kim JH, Bong SS, Heung SK, Lee YJ, Min SK, Daseul J, Zafar A, Jaehwan K (2015) Review of nanocellulose for sustainable future materials. Int J Precis Eng Manuf Green Technol 2:197–213. https://doi.org/10.1007/s40684-015-0024-9
- Lai EP, Wong B, Vandernoot VA (1993) Preservation of solid mercuric dithizonate samples with polyvinyl chloride for determination of mercury(II) in environmental waters by photochromism-induced photoacoustic spectrometry. Talanta 40:1097–1105. https://doi.org/10.1016/0039-9140(93)80172-N
- Larson KA, John MW (1992) Liquid ion exchange for mercury removal from water over a wide pH range. Ind Eng Chem Res 31:2714–2722. https://doi.org/10.1021/ie00012a013
- Liu P, Kristiina O, Aji PM (2016) Surface adsorption and selfassembly of Cu(II) ions on TEMPO-oxidized cellulose nanofibers in aqueous media. J Colloid Interface Sci 464:175–182. https://doi.org/10.1016/j.jcis.2015.11.033
- Masruchin N, Kurniawan Y, Sukma K, Putri A, Lisman S, Arif N (2019) TEMPO-mediated oxidation cellulose pulp modified with Monosodium Glutamate (MSG). IOP Conf Ser Earth Environ Sci 374:012010. https://doi.org/10.1088/1755-1315/374/1/012010
- Melesse A, Berihun K (2013) Chemical and mineral compositions of pods of Moringa stenopetala and Moringa oleifera cultivated in the lowland of Gamogofa Zone. J Environ Occup Sci 2:33–38. https://doi.org/10.5455/jeos. 20130212090940
- Mohadesi A, Mehdi R, Hosseinpour-Mashkani SM (2014) Solvent-free synthesis of mercury oxide nanoparticles by a



- simple thermal decomposition method. Superlattices Microstruct 66:48–53. https://doi.org/10.1016/j.spmi. 2013.11.017
- Nam KH, Sergio GS, Lawrence LT (2003) Mercury(II) adsorption from wastewaters using a thiol functional adsorbent. Ind Eng Chem Res 42:1955–1964. https://doi. org/10.1021/ie0208341
- Ornaghi J, Heitor L, Ademir JZ, Sandro CA (2014) Thermal behavior and the compensation effect of vegetal fibers. Cellulose 21:189–201. https://doi.org/10.1007/s10570-013-0126-x
- Puanngam M, Unob F (2008) Preparation and use of chemically modified MCM-41 and silica gel as selective adsorbents for Hg(II) ions. J Hazard Mater 154:578–587. https://doi.org/10.1016/j.jhazmat.2007.10.090
- Rio S, Delebarre A (2003) Removal of mercury in aqueous solution by fluidized bed plant fly ash. Fuel 82:153–159. https://doi.org/10.1016/S0016-2361(02)00237-5
- Sajjadi SA, Alireza M, Hai NT, Ioannis A, Guilherme LD, Zorica RL, Selvaraju S, Abolfazl RS, Andrei I, Ahmad HB (2018) Efficient mercury removal from wastewater by pistachio wood wastes-derived activated carbon prepared by chemical activation using a novel activating agent. J Environ Manag 223:1001–1009. https://doi.org/10.1016/ j.jenvman.2018.06.077
- Sehaqui H, Andreas M, Uxua PL, Numa P, Philippe T, Tanja Z (2016) Cationic cellulose nanofibers from waste pulp residues and their nitrate, fluoride, sulphate and phosphate adsorption properties. Carbohydr Polym 135:334–340. https://doi.org/10.1016/j.carbpol.2015.08.091
- Sharma PR, Aurnov C, Chengbo Z, Sunil KS, Lihong G, Benjamin SH (2018a) Lead removal from water using carboxycellulose nanofibers prepared by nitro-oxidation method. Cellulose 25:1961–1973. https://doi.org/10.1007/s10570-018-1659-9
- Sharma PR, Aurnov C, Sunil KS, Lihong G, Nasim A, Darren M, Benjamin SH (2018b) Nanocellulose from spinifex as an effective adsorbent to remove Cadmium(II) from water. ACS Sustain Chem Eng 6:3279–3290. https://doi.org/10.1021/acssuschemeng.7b03473
- Sharma PR, Aurnov C, Sunil KS, Benjamin SH (2017a) Efficient removal of UO₂²⁺ from water using carboxycellulose nanofibers prepared by the Nitro-Oxidation method. Ind Eng Chem Res 56:13885–13893. https://doi.org/10.1021/acs.iecr.7b03659
- Sharma PR, Ritika J, Sunil KS, Benjamin SH (2017b) A simple approach to prepare carboxycellulose nanofibers from untreated biomass. Biomacromol 18:2333–2342. https:// doi.org/10.1021/acs.biomac.7b00544
- Sharma PR, Sunil KS, William B, Hui C, Benjamin SH (2020a) Remediation of UO₂²⁺from water by Nitro-Oxidized carboxycellulose nanofibers: performance and mechanism. In: Contaminants in our water: identification and remediation methods. ACS, pp 269–283. https://doi.org/10.1021/bk-2020-1352.ch013
- Sharma PR, Varma AJ (2014a) Functionalized celluloses and their nanoparticles: morphology, thermal properties, and solubility studies. Carbohydr Polym 104:135–142. https:// doi.org/10.1016/j.carbpol.2014.01.015
- Sharma PR, Varma AJ (2014b) Thermal stability of cellulose and their nanoparticles: effect of incremental increases in

- carboxyl and aldehyde groups. Carbohydr Polym 114:339–343. https://doi.org/10.1016/j.carbpol.2014.08. 032
- Sharma PR, Bingqian Z, Sunil KS, Chengbo Z, Ruifu W, Surita RB, Benjamin SH (2018c) High aspect ratio carboxycellulose nanofibers prepared by Nitro-Oxidation method and their nanopaper properties. ACS Appl Nano Mater 1:3969–3980. https://doi.org/10.1021/acsanm.8b00744
- Sharma SK, Priyanka RS, Hui C, Ken J, Chengbo Z, Ruifu W, Benjamin H (2020b) Cellulose-supported nanosized zinc oxide: highly efficient bionanomaterial for removal of arsenic from water. In: Contaminants in Our Water: Identification and Remediation Methods. ACS, pp 253–267. https://doi.org/10.1021/bk-2020-1352.ch012
- Sharma SK, Priyanka RS, Simon L, Hui C, Ken J, Ruifu W, William B, Chengbo Z, Benjamin SH (2020c) Reinforcement of natural rubber latex using jute carboxycellulose nanofibers extracted using Nitro-Oxidation method. Nanomaterials 10:706. https://doi.org/10.3390/nano10040706
- Skubal LR, Meshkov NK (2002) Reduction and removal of mercury from water using arginine-modified TiO₂. J Photochem Photobiol A 148:211–214. https://doi.org/10.1016/S1010-6030(02)00045-X
- Sluiter A, Hames B, Ruiz R, Scarlata C, Sluiter J, Templeton D, Crocker D (2010) Determination of structural carbohydrates and lignin in biomass. https://www.nrel.gov/docs/ gen/fy13/42618.pdf. Issue Date: April 2008
- Strojny EJ, Iwamasa RT, Ludo KF (1971) Oxidation of 2-methoxyethanol to methoxyacetic acid by nitric acid solutions. JACS 93:1171–1178. https://doi.org/10.1021/ja00734a024
- Suman AK, Meeta G, Jain VK (2015) A novel reusable nanocomposite for complete removal of dyes, heavy metals and microbial load from water based on nanocellulose and silver nano-embedded pebbles. Environ Technol 36:706–714. https://doi.org/10.1080/09593330.2014. 959066
- Thakur VK, Voicu SI (2016) Recent advances in cellulose and chitosan based membranes for water purification: a concise review. Carbohydr Polym 146:148–165. https://doi.org/10.1016/j.carbpol.2016.03.030
- Tran L, Pingxiao W, Yajie Z, Shuai L, Nengwu Z (2015) Comparative study of Hg(II) adsorption by thiol- and hydroxyl-containing bifunctional montmorillonite and vermiculite. Appl Surf Sci 356:91–101. https://doi.org/10. 1016/j.apsusc.2015.08.038
- Wang D (2019) A critical review of cellulose-based nanomaterials for water purification in industrial processes. Cellulose 26:687. https://doi.org/10.1007/s10570-018-2143-2
- Wang JW, Kuo YM (2007) Preparation of fructose-mediated (polyethylene glycol/chitosan) membrane and adsorption of heavy metal ions. J Appl Polym Sci 105:1480–1489. https://doi.org/10.1002/app.26379
- Wang R, Sihui G, Anna S, Xiao W, Zhe W, Rui Y, Benjamin SH, Benjamin C (2013) Nanofibrous microfiltration membranes capable of removing bacteria, viruses and heavy metal ions. J Membr Sci 446:376–382. https://doi.org/10.1016/j.memsci.2013.06.020



Wang X, Andrews L (2005) Infrared spectrum of Hg(OH)₂ in solid neon and argon. Inorg Chem 44:108–113. https://doi.org/10.1021/ic048673w

- Zabihi M, Ahmadpour A, Haghighi AA (2009) Removal of mercury from water by carbonaceous sorbents derived from walnut shell. J Hazard Mater 167:230–236. https://doi.org/10.1016/j.jhazmat.2008.12.108
- Zhang FS, Jerome ON, Hideaki I (2005) Mercury removal from water using activated carbons derived from organic sewage sludge. Water Res 39:389–395. https://doi.org/10.1016/j.watres.2004.09.027
- Zhang X, Zhihai Z, Guangjun R, Yan L, Shuang L, Bing Z, Zichen W (2013) Synthesis of lignin-modified silica

- nanoparticles from black liquor of rice straw pulping. Powder Technol 246:664–668. https://doi.org/10.1016/j.powtec.2013.06.034
- Zhu C, Illia D, Jens R, Sven O, Allan H, Aji PM (2015) Adsorption behavior of cellulose and its derivatives toward Ag(I) in aqueous medium: an AFM, spectroscopic, and DFT study. Langmuir 31:12390–12400. https://doi.org/10. 1021/acs.langmuir.5b03228

Publisher's Note Springer Nature remains neutral with regard to jurisdictional claims in published maps and institutional affiliations.

